Proceedings of the ASME 2014 International Design Engineering Technical Conferences & Computers and Information in Engineering Conference
IDETC/CIE 2014
August 17-20, 2014, Buffalo, New York, USA

DETC2014-34516

ON THE THERMOMECHANICAL RESPONSE OF HTPB COMPOSITE BEAMS UNDER NEAR-RESONANT BASE EXCITATION

Daniel C. Woods, Jacob K. Miller, and Jeffrey F. Rhoads*
School of Mechanical Engineering,
Birck Nanotechnology Center,
and Ray W. Herrick Laboratories
Purdue University
West Lafayette, Indiana 47907
Email: jfrhoads@purdue.edu

ABSTRACT

Currently, there is a pressing need to detect and identify explosive materials in both military and civilian settings. While these energetic materials vary widely in both form and composition, many traditional explosives consist of a polymeric binder material with embedded energetic crystals. Interestingly, many polymers exhibit considerable self-heating when subjected to harmonic loading, and the vapor pressures of many explosives exhibit a strong dependence on temperature. In light of these facts, thermomechanics represent an intriguing pathway for the stand-off detection of explosives, as the thermal signatures attributable to motion-induced heating may allow target energetic materials to be distinguished from their more innocuous counterparts. In the present work, the mechanical response of a polymeric particulate composite beam subjected to near-resonant base excitation is modeled using Euler-Bernoulli beam theory. Significant sources of heat generation are identified and used with distributed thermal models to characterize the system's thermomechanical response. In addition, the results of experiments conducted using a hydroxyl-terminated polybutadiene (HTPB) beam with embedded ammonium chloride (NH_4Cl) crystals are presented. The thermal and mechanical responses of the sample are recorded using infrared thermography and scanning laser Doppler vibrometry, and subsequently compared to the work's analytical findings. By adopting the combined research approach utilized herein, the authors seek to build upon recent work and bridge the considerable gap that exists between theory and experiments in this specific field. To this end, the authors hope that this work will represent an integral step in enhancing the ability to successfully detect explosive materials.

1 INTRODUCTION

To address matters of security in military and civilian settings, there is, at present, a significant need for new technologies capable of detecting explosive materials. Though there is a wide variety of detection systems currently in use, many exploit the volatility of energetic materials and detect the saturated vapors that exist near the materials' surfaces [1, 2]. Unfortunately, vapor pressures drop significantly if the explosive materials are sealed or packed in a bag, or both, which is often the case [3]. These pressures also drop considerably in certain environments, such as with strong winds and at lower temperatures [3]. As such, trace vapor detection of improvised explosive devices (IEDs) remains a substantial technical challenge.

Given the strong dependence of vapor pressure on temperature, explosive detection capabilities may be significantly enhanced by heating the target material. Though energetic materials vary widely in form and composition, many traditional explosives consist of a polymeric binder material with embedded energetic crystals. Polymers exhibit considerable self-heating when

*Address all correspondence to this author.

subjected to harmonic loading, owing to distinctly out-of-phase stress and strain oscillations [4]. In addition, low-frequency mechanical and acoustic excitations can be transmitted over relatively large distances, allowing for stand-off excitation. Taken collectively, these seemingly disparate statements suggest that thermomechanics may provide an intriguing pathway for explosives detection, as the self-heating response of explosive materials to low-frequency excitation may be exploited to increase vapor pressure from a stand-off distance, and thus increase the relative utility of vapor-based detection systems.

Heat generation in response to mechanical or acoustic excitation is well-documented for pure materials and composites. Thermomechanical coupling is described by the thermodynamic theory of solids, which is inclusive of both viscoelastic and thermoelastic effects [6]. Thermal responses to acoustic and ultrasonic excitation are commonly exploited in the field of vibrothermography [7–11] to identify defects in structures and samples by nondestructive means. Such identifications are enabled by the fact that thermal responses are particularly exacerbated near stress concentrations.

Thermal responses are also elicited when materials are subjected to mechanical or acoustic excitation due to material damping. Dimarogonas and Syrimbeis [12], for example, considered the heat generated in vibrating rectangular plates due to bulk material damping. The related self-heating effect was documented in polymeric materials in the seminal studies by Ratner and Korobov [4, 5] and in more recent experiments [13–16], amongst other places. In the area of polymeric composites, Katunin and Fidali [13, 14] conducted experiments using glass fiber-reinforced laminate plates and proposed models of the self-heating effect. In addition, the thermal and mechanical responses of particulate composite plates subjected to direct mechanical excitation were examined in [16]. The particle/binder ratio of particulate composites is known to have a strong impact on material properties [17–20], and the influence of this ratio on the thermal and mechanical responses was considered in [16] as well. In explosive materials, the works of Loginov [21, 22] provide insight into the nature of the heating of explosives subjected to mechanical excitation. However, these studies are largely phenomenological in nature and do not focus on heating achieved through frequency-selective excitation.

The aim of this paper is to characterize the thermomechanical response of a polymeric particulate composite material subjected to mechanical excitation, with an eye towards explosives detection. To this end, the mechanical response of a polymeric particulate composite beam subjected to harmonic excitation is modeled using Euler-Bernoulli beam theory. A macroscale model of the polymer composite as a homogenized linear viscoelastic material is considered. Significant sources of heat generation are identified and used with distributed thermal models to characterize the thermomechanical response of the system. This effort builds upon past work by Senchenkov and Karnaukhov [23–25], which presented constitutive relations for viscoelastic materials under harmonic loading, and Dinzart and Molinari [26], which modeled the thermomechanical response of a viscoelastic beam under harmonic bending, considering only heat transfer in the transverse direction, though here heat transfer in all three dimensions is taken into account. With the goal of maximizing self-heating for the application of trace vapor detection, near-resonant excitations are considered. In addition, the results of experiments conducted using a hydroxyl-terminated polybutadiene (HTPB) beam with embedded ammonium chloride (NH_4Cl) crystals are presented. The sample composition, also used in [16], is a mock mechanical material intended to resemble a common propellant or plastic-bonded explosive. The thermal and mechanical responses of the sample are recorded using infrared thermography and scanning laser Doppler vibrometry, and subsequently compared to the work's analytical findings. Through the use of this combined research approach, the authors seek to build upon recent work and bridge the considerable gap that currently exists between theory and experiments in this specific field.

2 VISCOELASTIC BEHAVIOR OF POLYMERS SUBJECTED TO HARMONIC EXCITATION

Polymers subjected to time-varying loading can be described by a viscoelastic model [27–29]. In general form, the stress-strain relationship for linear viscoelastic materials involves successive time derivatives of both stress and strain [29], according to

$$a_0\sigma + a_1\frac{\mathrm{d}\sigma}{\mathrm{d}t} + a_2\frac{\mathrm{d}^2\sigma}{\mathrm{d}t^2} + ... = b_0\varepsilon + b_1\frac{\mathrm{d}\varepsilon}{\mathrm{d}t} + b_2\frac{\mathrm{d}^2\varepsilon}{\mathrm{d}t^2} + ... \quad (1)$$

where $\sigma(t)$ and $\varepsilon(t)$ are the stress and strain histories, respectively, and the a_i and b_i are material parameters.

Though the representation as a differential equation is general, a more convenient approach is the hereditary integral method, attributed to Boltzmann [30]. According to the Boltzmann superposition principle, the stress-strain relationship can be expressed as [29]

$$\sigma(t) = \int_{-\infty}^{t} R(t-\tau)\frac{\mathrm{d}\varepsilon}{\mathrm{d}\tau}\mathrm{d}\tau \quad (2)$$

where R is the relaxation kernel, τ is the relaxation time, and the lower limit of negative infinity indicates that all previous events, including, for example, production processes, should be included in the stress analysis for polymer structures.

With the assumption of harmonic loading, stress and strain

can be approximated as

$$\sigma = \sigma_0 e^{i\omega t + i\delta(\omega)}$$
$$\varepsilon = \varepsilon_0 e^{i\omega t} \tag{3}$$

where σ_0 and ε_0 are the stress and strain amplitudes, respectively, ω is the angular frequency, and δ is the phase difference between the stress and strain. The complex dynamic modulus representation [28] follows from this approximation as

$$E^*(\omega) = E'(\omega) + iE''(\omega) = |E^*(\omega)|e^{i\delta(\omega)} \tag{4}$$

where E^* is the complex modulus, E' is the storage modulus (associated with elastic behavior), and E'' is the loss modulus (associated with dissipative behavior). The material loss factor, η, is defined as the ratio of the loss modulus to the storage modulus: $\eta = E''/E' = \tan(\delta)$. The complex dynamic modulus is related to the relaxation kernel through the Fourier transform [29]

$$E^*(\omega) = i\omega \int_0^\infty R(t) e^{-i\omega t} \mathrm{d}t \tag{5}$$

Also taking into account the temperature-dependence of the dynamic modulus, the stress-strain relationship is given by

$$\sigma(t) = E^*(\omega, \theta)\varepsilon(t) \tag{6}$$

where θ represents the temperature of the material as measured from ambient [29].

Thermomechanical coupling in polymers is due to both reversible thermoelastic effects and internal energy dissipation. Experiments show that under intensive loading, the dominant mechanism in polymers is internal dissipation [25], generally described by a viscoelastic model. During harmonic loading, the energy losses caused by out-of-phase oscillations between stress and strain generate heat [14]. Due to the poor thermal conductivity of most polymers, this leads to considerable self-heating. That is, the temperature of the polymer rises until a thermal steady state is reached, at which point the heat dispelled to the environment balances that generated from dissipation. Thermal runaway is also possible [26].

3 MODELING OF A THIN POLYMER-BASED BEAM SUBJECTED TO HARMONIC EXCITATION

3.1 EQUATION OF MOTION

The polymeric particulate composite material of interest here is modeled as a homogenized linear viscoelastic material. The utilized x-axis is defined along the beam axis at the centroid of the cross-section, and the y- and z-axes are as shown in Fig. 1. The exact geometry of the rectangular beam is also prescribed in the figure. The beam is subjected to harmonic excitation in the transverse, y, direction.

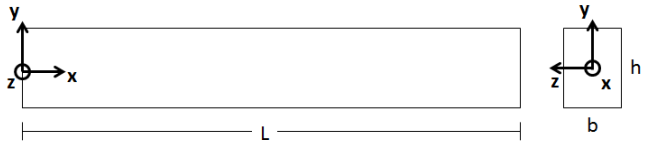

FIGURE 1. AN UNDEFORMED RECTANGULAR BEAM.

The standard assumptions of Euler-Bernoulli beam theory are used. Namely, effects due to shear deformation and rotary inertia are neglected [31]. The equation for transverse motion is thus given by

$$D^*(\omega, \theta)\frac{\partial^4 u}{\partial x^4} + \rho h \frac{\partial^2 u}{\partial t^2} = f^* \tag{7}$$

where, using complex quantities where appropriate, u is the transverse displacement of the neutral surface, ρ is the mass density, f^* is the forcing function per unit area, and D^* is the flexural rigidity, which is given by [31]

$$D^*(\omega, \theta) = \frac{E^*(\omega, \theta)h^3}{12[1 - \nu^2(\omega, \theta)]} \tag{8}$$

where ν is Poisson's ratio. For beams with a considerable aspect ratio (b/h), the effective stiffness is increased due to the two-dimensional effect in the xz-plane, as in plate-like bending [31, 32]. Accordingly, the flexural rigidity for a thin plate is used, which accounts for the effect of Poisson's ratio on the flexural stiffness.

Considered here is the case for which the ends of the beam, $x = 0$ and $x = L$, are subjected to a harmonic acceleration, $Ae^{i\omega t}$. The suspended beam is then under inertial excitation with the complex forcing function f^* set to zero. The transverse displacement is assumed to have the form

$$u(x,t) = \frac{A}{\omega^2} e^{i\omega t} + \tilde{u}(x,t) \tag{9}$$

where $\tilde{u}$ is the relative deflection of the beam resulting from the base excitation $\frac{A}{\omega^2} e^{i\omega t}$. The equation for transverse motion be-

comes

$$D^*(\omega,\theta)\frac{\partial^4\tilde{u}}{\partial x^4}+\rho h\frac{\partial^2\tilde{u}}{\partial t^2}=\rho hAe^{i\omega t} \tag{10}$$

For a beam clamped on both ends, the boundary conditions are given by

$$\begin{aligned}\tilde{u}|_{x=0}&=\frac{\partial\tilde{u}}{\partial x}|_{x=0}=0\\ \tilde{u}|_{x=L}&=\frac{\partial\tilde{u}}{\partial x}|_{x=L}=0\end{aligned} \tag{11}$$

Using the normal mode approach [31], the steady-state displacement is

$$\tilde{u}(x,t)=\sum_{n=1}^{\infty}U_n(x)\frac{\rho hA\int_0^L U_n(x)\mathrm{d}x}{D^*(\omega,\theta)\beta_n^4-\rho h\omega^2}e^{i\omega t} \tag{12}$$

where U_n are the mode shapes that satisfy the boundary conditions provided in Eq. (11), which are given by [31]

$$\begin{aligned}U_n(x)=C_n\big[&\cos(\beta_n x)-\cosh(\beta_n x)\\&-\frac{\cos(\beta_n L)-\cosh(\beta_n L)}{\sin(\beta_n L)-\sinh(\beta_n L)}\left(\sin(\beta_n x)-\sinh(\beta_n x)\right)\big];\\&n=1,2,3,...\end{aligned} \tag{13}$$

and where the constants C_n are given according to the normalization condition

$$\int_0^L U_n^2\mathrm{d}x=1 \tag{14}$$

The constants β_n are the n^{th} positive roots of the corresponding characteristic equation [31]

$$\cos(\beta_n L)\cosh(\beta_n L)-1=0 \tag{15}$$

3.2 HEAT TRANSFER EQUATION

Given that the polymer composite is modeled as a homogenized linear viscoelastic material, thermal isotropy is assumed as well. In addition, the material's thermal properties are modeled as constant and the effects of thermal expansion are neglected for the small temperature fluctuations considered. Using the Fourier Law of Conduction and considering heat diffusion in all three dimensions, the heat transfer equation is [33]

$$\frac{\partial^2\theta}{\partial x^2}+\frac{\partial^2\theta}{\partial y^2}+\frac{\partial^2\theta}{\partial z^2}+\frac{1}{k}r=\frac{1}{\alpha}\frac{\partial\theta}{\partial t} \tag{16}$$

where k is the thermal conductivity, α is the thermal diffusivity, and r is the volumetric energy generation.

A Green's function approach [34] can be employed to analytically solve the transient heat transfer equation highlighted above. Specifically, the Green's function for a given geometry and set of boundary conditions can be used to construct the temperature solution in conjunction with spatially- and temporally-dependent volumetric energy generation terms [34]. However, even one-dimensional Green's functions typically involve infinite summations, and two- and three-dimensional Green's functions for a rectangular coordinate system use the product of the one-dimensional infinite summations [34]. In addition, spatially-dependent volumetric energy generation is difficult to incorporate analytically in a convenient way, and the aforementioned summations tend to converge slowly [34]. Alternate basis functions, including the beam's mode shapes, have been explored, but convergence issues likewise hamper the utility of these analytical approaches. As such, the volumetric energy generation is computed analytically here and used in conjunction with numerical methods to recover the predicted temperature distributions.

The mechanical energy dissipated in the beam per cycle of harmonic loading can be approximated as the area under the hysteresis loop of the stress-strain plot in the mechanical steady state [29]. Assuming that the temperature varies on a much slower order than the mechanical loading, the volumetric energy generation can be time-averaged over one mechanical loading cycle [26]. If the energy is dissipated solely as heat, then the time-averaged volumetric energy generation is given by

$$\begin{aligned}r_{avg}&=\frac{\omega}{2\pi}\int_{t_0}^{t_0+2\pi/\omega}\sigma\frac{\partial\varepsilon}{\partial\tau}\mathrm{d}\tau\\&=\frac{E'\eta\omega\varepsilon_0^2}{2(1-\nu^2)}\end{aligned} \tag{17}$$

In Euler-Bernoulli beam theory, the strain magnitude depends on the transverse position, y, and on the curvature of the neutral surface [35], according to

$$\varepsilon_0(x,y)=-y\kappa_0(x) \tag{18}$$

where $\kappa_0(x)$ is the maximum value of the curvature, computed

using the second spatial derivative

$$\kappa_0(x) = \max\left[\frac{\partial^2 \tilde{u}(x,t)}{\partial x^2}\right]; \quad t \in [t_0, t_0 + 2\pi/\omega] \tag{19}$$

For a thin beam, the volumetric energy generation can also be spatially-averaged over the thickness [12]. This gives the one-dimensional heat source

$$r(x) = \frac{E'\eta\omega h^2}{24(1-\nu^2)}\kappa_0^2(x) \tag{20}$$

If a thermal steady state is reached, the heat lost to the environment balances that generated from dissipation, though thermal runaway can occur, for example in materials with sufficiently poor thermal conductivity [26]. In this work, the transient temperature behavior is investigated in two- and three-dimensional numerical simulations using the heat source given in Eq. (20).

4 EXPERIMENTAL STUDY OF A PARTICULATE COMPOSITE BEAM

Experiments were conducted using an HTPB beam with embedded NH_4Cl crystals. These ammonium chloride crystals were selected to approximate the particle sizes of ammonium perchlorate (AP), and, as such, the sample serves as a mechanical mock material for a common propellant or plastic-bonded explosive. The thermal and mechanical responses of the sample were recorded using infrared thermography and scanning laser Doppler vibrometry, as subsequently described.

4.1 SAMPLE PREPARATION

To create the experimental sample, powder-form HTPB was heated to 60°C and allowed to harden using an isocyanate agent. For mixing with the NH_4Cl crystals, a wetting agent, Tepanol, was applied and a Resodyn acoustic mixer was used to ensure homogeneity. The mixture, designed to be 75% NH_4Cl by volume, was poured into a purpose-built plate mold and cured overnight, and then cut into a beam measuring 25.6 x 2.5 x 1.4 cm. The density of the beam was computed from direct length and mass measurements as 1028.2 kg/m^3. This density is significantly lower than what would be predicted by a linear mix of the densities of pure HTPB and crystalline NH_4Cl, a discrepancy likely attributable to voids in the mixture.

4.2 EXPERIMENTAL SETUP

A TIRA 59335/LS AIT-440 electrodynamic shaker was used to provide mechanical excitation to the beam, allowing for band-limited white noise or single-frequency harmonic inertial excitation. A VibeLab VL-144 vibration control system was employed to control the system through direct monitoring of an accelerometer mounted on the shaker head. The beam was attached to the shaker using a custom fixture, which was machined to simulate clamped boundaries on both short ends of the beam. The final mounting yielded a 22.9 cm (9 in) unsupported length. The frequency responses and operational deflection shapes of the beam were recorded using a Polytec PSV-400 scanning laser Doppler vibrometer. The test sample and experimental apparatus are shown in Fig. 2.

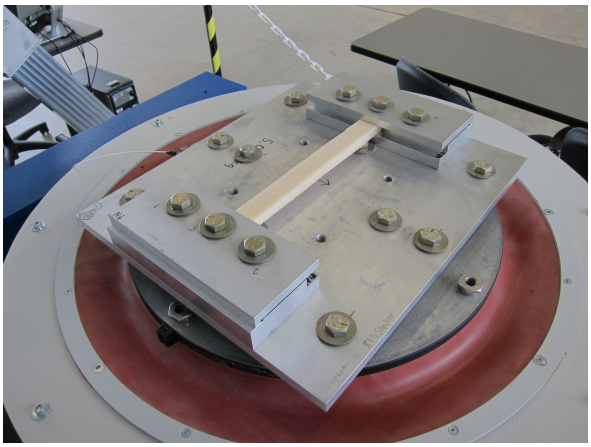

FIGURE 2. THE EXPERIMENTAL SAMPLE, AN HTPB BEAM WITH EMBEDDED NH_4Cl CRYSTALS, MOUNTED ON A TIRA 59335/LS AIT-440 ELECTRODYNAMIC SHAKER.

For the purposes of mechanical analysis, broadband (10-1000 Hz) white noise excitation was applied at three forcing levels (1, 1.86, and 2.44 g RMS). The system response was estimated using the classical H1 estimator, which compares the measured cross-spectral density of the accelerometer and vibrometer readings to the measured power spectral density of the accelerometer. The H1 frequency response estimators were calculated at two distinct points, the geometric center of the top face of the beam and an offset point on the top face, for all three forcing levels. The offset point was located one quarter of the distance along the beam, on the centerline.

The transient and steady-state thermal responses of the top face were recorded using a FLIR A325 thermal camera, which has a temperature sensitivity of 0.07°C at 30°C and an accuracy of ±2°C or ±2%. The infrared data was calibrated to the emissivity of the beam using a thermocouple at ambient conditions. For thermal testing, the beam was excited near first resonance for 60 minutes and was seen to approach thermal steady state within this time. Though no attempt was made to control the ambient

temperature or flow conditions, neither was observed to change significantly for the duration of the experiment.

5 NUMERICAL SIMULATION

To solve the heat transfer equation highlighted above, numerical methods were employed. First, an in-house Mathematica code was utilized to compute the mechanical response of the beam and numerically solve the two-dimensional problem of heat diffusion in the *xz*-plane using the heat source given in Eq. (20). For the mechanical portion of the simulation, the density value was specified as 1028.2 kg/m^3, as obtained from direct measurement. The Poisson's ratio was estimated as 0.39, based on perceived similarities to more common materials. The storage modulus was estimated from the resonant response of a cylindrical sample of the same HTPB composite as 83.57 MPa [36]. The material loss factor was estimated as 0.35 by using the half-power bandwidth method on data taken from experimental frequency responses [37].

To solve the heat equation, the thermal conductivity and thermal diffusivity were measured using the transient plane source technique [38] as 0.52 W/(m-K) and 3.13×10^{-7} m^2/s, respectively. For the two-dimensional Mathematica solution, a stiffness switching method was employed. A convective heat sink was applied to the two-dimensional surface, using a convection coefficient of 5 W/(m^2-K) in an attempt to match the transient behavior observed experimentally. This value is comparable with coefficients found in experimental investigations [39–41] and is within the range for free convection estimates presented in [33]. Insulated boundary conditions were applied on all edges. An additional three-dimensional finite element simulation, implemented in COMSOL, was employed as a further point of comparison. In this simulation, the same heat source was applied to a 259-node three-dimensional mesh with insulated boundary conditions on the ends and convective conditions elsewhere. Both methods were used to generate simulations of transient behavior over 60 minutes, as well as top-down thermal profiles, which allow for direct comparison to the experimentally-obtained thermal images.

6 RESULTS AND DISCUSSION

6.1 MECHANICAL RESPONSE

The H1 frequency response estimators for the beam in response to the three levels of band-limited white noise excitation are presented as Fig. 3. Data at both the center and offset points on the top face are presented. The beam exhibits multiple clear resonant peaks, which decrease slightly in relative amplitude and frequency as the forcing level increases.

The beam was also excited with harmonic forcing at the first resonant frequency, which was estimated from the H1 frequency response estimators for each of the respective forcing levels. A representative operational deflection shape recorded at 2g harmonic forcing is presented with the theoretically-recovered magnitude of steady-state displacement in Fig. 4. As is evident from the figure, the system model approximates the behavior of the particulate composite to an acceptable degree. The magnitudes of the experimentally-recorded displacements show good agreement with the theoretical predictions. For example, in the representative operational deflection shape shown in Fig. 4, there is a 4.5% error in the measured response compared to the theoretical prediction at the center of the beam. Due to the imperfect nature of the clamping fixture, there are notable deviations at the ends, resulting in higher local predicted stresses as compared to the stresses encountered in the experiment. These deviations may also be attributable to the fact that the scanning laser Doppler vibrometer had difficulty in measuring the response near the clamping fixture.

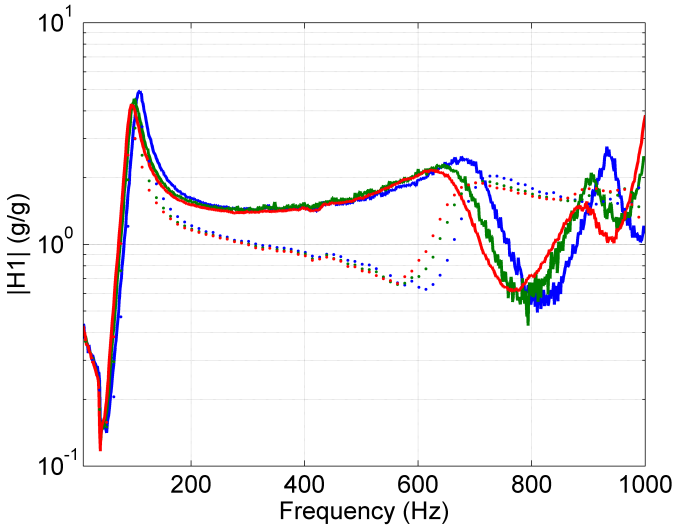

FIGURE 3. THE EXPERIMENTAL H1 MECHANICAL FREQUENCY RESPONSE ESTIMATORS FOR THREE LEVELS OF EXCITATION. THE BLUE, GREEN, AND RED CURVES REPRESENT RESPONSES AT 1, 1.86, AND 2.44 g RMS, RESPECTIVELY. SOLID LINES CORRESPOND TO DATA FROM THE CENTER POINT AND DASHED LINES CORRESPOND TO DATA FROM THE OFFSET POINT.

6.2 THERMAL RESPONSE

With the beam excited with 1g, 2g, and 3g harmonic forcing near the first natural frequency, the transient thermal response of the top surface was recorded. The recorded maximum and mean transient surface temperatures are presented as Fig. 5. Due to the intrinsic noise in infrared temperature measurement, the data points presented represent the average of five temporally-adjacent thermal measurements. For each of the forcing levels,

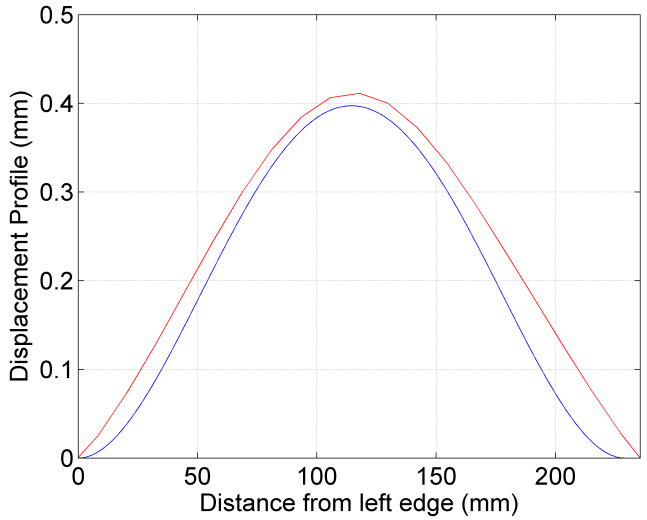

FIGURE 4. A REPRESENTATIVE OPERATIONAL DEFLECTION SHAPE RECORDED AT 2g HARMONIC FORCING NEAR THE BEAM'S FIRST NATURAL FREQUENCY (RED CURVE) PLOTTED WITH THE THEORETICAL MAGNITUDE OF STEADY-STATE DISPLACEMENT (BLUE CURVE).

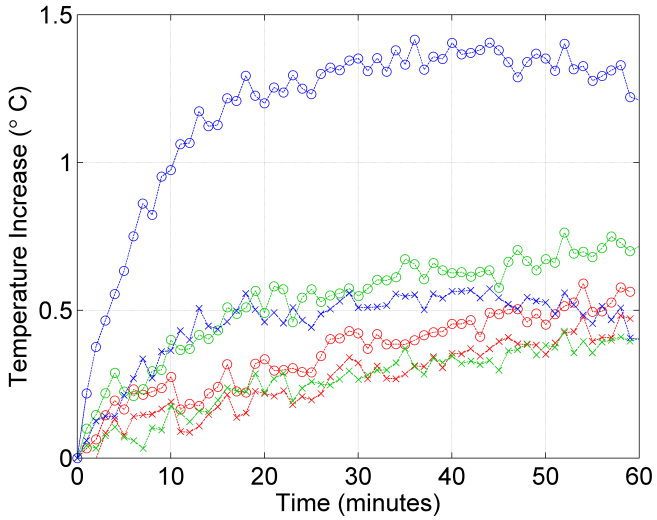

FIGURE 5. THE EXPERIMENTAL MAXIMUM AND MEAN TRANSIENT SURFACE TEMPERATURES OBTAINED WITH HARMONIC FORCING NEAR THE FIRST NATURAL FREQUENCY. THE RED, GREEN, AND BLUE DATA POINTS REPRESENT RESPONSES TO FORCING AT 1g, 2g, AND 3g, RESPECTIVELY. CIRCLES CORRESPOND TO MAXIMUM SURFACE TEMPERATURES AND EXES CORRESPOND TO MEAN SURFACE TEMPERATURES.

the temperatures asymptotically approach steady-state values in the 60 minutes of recording time. In general, greater forcing levels lead to greater heating, and the maximum recorded surface temperatures increase with forcing level. The highest mean surface temperatures are for 3g forcing, though the recorded mean temperatures for 1g and 2g forcing are comparable. In addition, the largest separation between the maximum and mean temperatures was recorded for the 3g forcing.

The surface temperature distributions recorded after 60 minutes are presented in Fig. 6. Maximal heating was recorded near the center of the surface for all forcing levels. The axial variation of temperature is observed to coincide with the stress and strain fields expected with a linear viscoelastic material. As noted in Eq. (17), the volumetric heat generation is proportional to the square of the strain magnitude. This effect is especially prominent with the 2g and 3g forcing levels, where higher local temperatures are observed in areas of high local stress near the ends of the beam. Variations in temperature through the width of the beam are attributable to the convective boundaries on each surface. Specifically, heat is dispelled to the environment at the surfaces and greater temperatures are generated at the center, farthest away from those surfaces. The effects of the stress field and convective boundaries interact in the surface temperature distributions recorded. The lesser prominence of structure for the 1g forcing level is due to the comparatively-lower temperature deviations recovered.

The numerical simulation results for the maximum and mean transient surface temperatures at all three forcing levels are presented in Figs. 7 and 8 for the two- and three-dimensional simulations, respectively. Likewise, the steady-state surface temperature distributions recovered from the simulations for 3g harmonic excitation are presented in Figs. 9 and 10, again for the two- and three-dimensional simulations, respectively. The steady-state surface temperatures computed for 3g harmonic excitation were also averaged over the width of the beam and the profiles are presented as a function of axial position in Fig. 11. The experimental temperature recorded after 60 minutes at 3g harmonic forcing, likewise averaged over the width of the beam, is also shown in Fig. 11. The temperature magnitudes recovered from the three-dimensional simulation show reasonable agreement with the recorded distributions. Temperatures in the two-dimensional simulation are seen to approach the thermal steady state more slowly than do the temperatures in the three-dimensional simulation. This is attributable to the fact that since heat is only allowed to diffuse in two dimensions in the former case, internal diffusion and rejection of heat to the environment is less effective. This also accounts for the greater temperatures obtained in the two-dimensional simulation. The steady-state surface temperature distribution computed in the three-dimensional simulation shows a character consistent

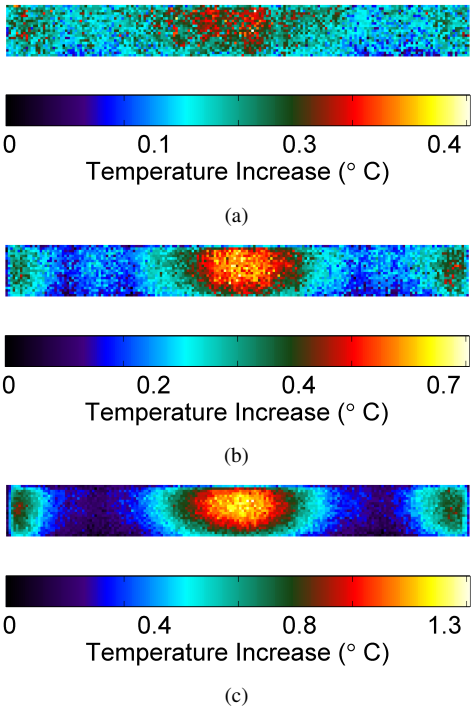

FIGURE 6. THE EXPERIMENTAL SURFACE TEMPERATURE DISTRIBUTION RECORDED AFTER 60 MINUTES IN RESPONSE TO HARMONIC FORCING AT: (a) 1g; (b) 2g; AND (c) 3g. FORCING WAS NEAR THE FIRST NATURAL FREQUENCY FOR EACH CASE.

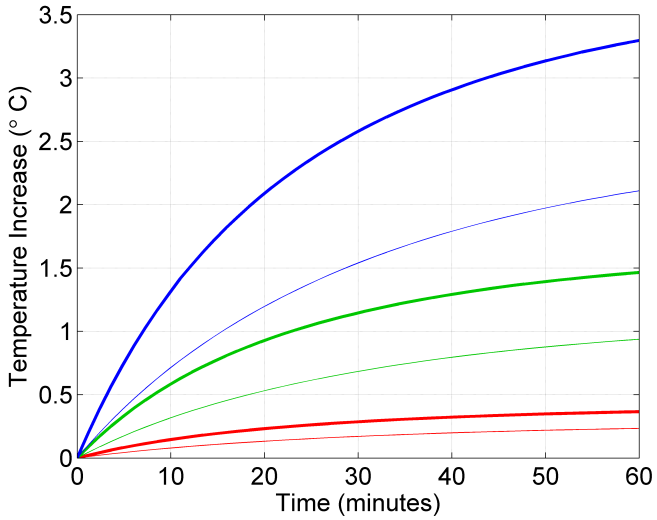

FIGURE 7. THE MAXIMUM AND MEAN TRANSIENT SURFACE TEMPERATURES OBTAINED IN THE TWO-DIMENSIONAL NUMERICAL SIMULATION WITH HARMONIC FORCING NEAR THE FIRST NATURAL FREQUENCY. THE RED, GREEN, AND BLUE CURVES REPRESENT RESPONSES TO FORCING AT 1g, 2g, AND 3g, RESPECTIVELY. BOLD LINES CORRESPOND TO MAXIMUM SURFACE TEMPERATURES AND THIN LINES CORRESPOND TO MEAN SURFACE TEMPERATURES.

with the distribution recorded at 3g forcing. A local region of higher temperatures is generated near the center and the effect of the convective boundaries is apparent at the edges. The simulation also captures the higher relative temperatures at the ends of the beam, but the observed effect is magnified as compared to experiments. As previously noted, this is likely due to the imperfect nature of the clamping fixture, which leads to higher predicted stresses near the ends of the beam when they are modeled as clamped boundaries.

7 CONCLUSIONS

A thermomechanical model of a polymeric particulate composite beam has been presented, wherein the composite is modeled as a homogenized linear viscoelastic material. The composition under consideration, which consists of an HTPB binder with embedded NH_4Cl crystals, is intended to resemble a common propellant or plastic-bonded explosive. Acquired results revealed a strong dependence of the thermal response on the stress and strain fields produced within the beam; and that internal heat generation is proportional to the square of the strain magnitude, as highlighted in Eq. (17). Numerical solvers were used with the derived heat source and yielded thermal responses consistent with those measured in experiments. In addition to modal structure, convection at the surfaces was shown to impact the thermal response, and temperature excursions were noted near the center of the beam geometry.

Since explosive vapor pressures exhibit a strong dependence on temperature, the capabilities of vapor-based detection systems may be enhanced significantly by heating. Heat generation in response to harmonic excitation increases, as noted, with strain magnitude and, for a given strain level, with forcing frequency. The strain magnitude may be increased with greater forcing levels or selective boundary conditions, though obviously there is limited control over boundary conditions in many explosives detection systems. Heat generation is also intensified as the phase difference between stress and strain oscillations, quantified by the material loss factor, is increased. The phase difference depends on the forcing level and frequency [28], and thus may be used to enhance heating. Though heating also depends on other moduli, there is little control over material properties and sample geometry in explosives detection applications. Low-frequency excitations can be transmitted over large distances, and thus may be used for stand-off heating, though the proportionality of heat generation to forcing frequency and the dependence of the stress-

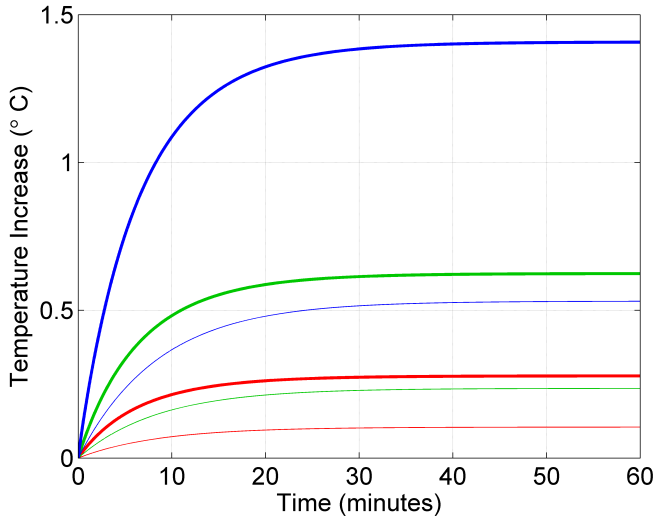

FIGURE 8. THE MAXIMUM AND MEAN TRANSIENT SURFACE TEMPERATURES OBTAINED IN THE THREE-DIMENSIONAL NUMERICAL SIMULATION WITH HARMONIC FORCING NEAR THE FIRST NATURAL FREQUENCY. THE RED, GREEN, AND BLUE CURVES REPRESENT RESPONSES TO FORCING AT 1g, 2g, AND 3g, RESPECTIVELY. BOLD LINES CORRESPOND TO MAXIMUM SURFACE TEMPERATURES AND THIN LINES CORRESPOND TO MEAN SURFACE TEMPERATURES.

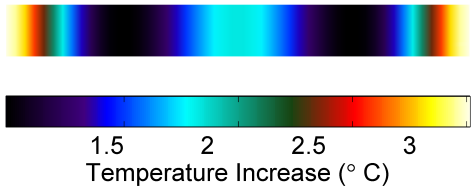

FIGURE 9. THE STEADY-STATE SURFACE TEMPERATURE DISTRIBUTION OBTAINED IN THE TWO-DIMENSIONAL NUMERICAL SIMULATION IN RESPONSE TO 3g HARMONIC FORCING NEAR THE FIRST NATURAL FREQUENCY.

strain phase lag would have to be considered in the design of an effective stand-off detection system.

In addition to the structural heating considered here, microscale heating of energetic materials through laser or ultrasonic excitation [15, 42, 43] may also constitute a viable pathway to improved trace vapor detection capabilities. Targeting local *hot spots* in the composite structure can result in greater thermal responses, but doing so generally requires proximal access to the material's surface.

Future work will attempt to optimize spatiotemporal inputs with an eye towards eliciting maximal thermal response in particulate composite materials, including explosives, for detection and inspection applications. This work will further investigate the thermomechanics of the composite materials, including structural and microscale heating, through theory and experimentation.

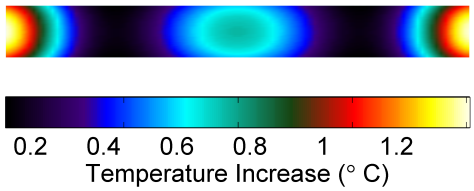

FIGURE 10. THE STEADY-STATE SURFACE TEMPERATURE DISTRIBUTION OBTAINED IN THE THREE-DIMENSIONAL NUMERICAL SIMULATION IN RESPONSE TO 3g HARMONIC FORCING NEAR THE FIRST NATURAL FREQUENCY.

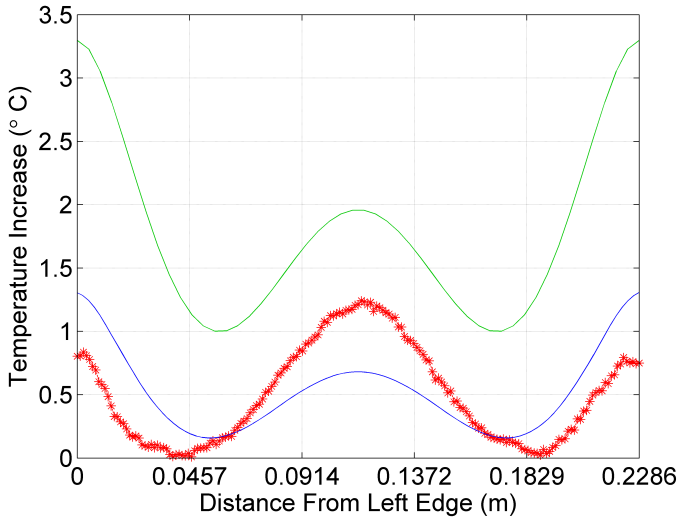

FIGURE 11. THE EXPERIMENTAL SURFACE TEMPERATURE DISTRIBUTION RECORDED AFTER 60 MINUTES AND THE STEADY-STATE SURFACE TEMPERATURE DISTRIBUTIONS OBTAINED IN NUMERICAL SIMULATIONS IN RESPONSE TO 3g HARMONIC FORCING NEAR THE FIRST NATURAL FREQUENCY. THE RED DATA POINTS CORRESPOND TO THE EXPERIMENTAL TEMPERATURES, AND THE GREEN AND BLUE CURVES CORRESPOND TO THE TWO- AND THREE-DIMENSIONAL NUMERICAL SIMULATIONS, RESPECTIVELY. THE TEMPERATURES ARE AVERAGED OVER THE BEAM WIDTH AT THE SURFACE AND PRESENTED AS A FUNCTION OF AXIAL POSITION.

ACKNOWLEDGEMENTS

This research is supported by the U.S. Office of Naval Research as a Multidisciplinary University Research Initiative on Sound and Electromagnetic Interacting Waves under ONR Grant No. N00014-10-1-0958. The authors would like to acknowledge Christopher Watson and Prof. Douglas Adams for their work in sample preparation, as well as Jelena Paripovic and Prof. Patricia Davies for mechanical property measurements and Jesus Mares, Prof. Lori Groven, and Prof. Steven Son for thermal property measurements. The authors would also like to acknowledge Prof. Timothy Fisher for valuable advice on analytical methods for heat conduction.

REFERENCES

[1] Moore, D. S., 2004. "Instrumentation for trace detection of high explosives". *Review of Scientific Instruments,* ***75***(8), pp. 2499–2512.

[2] Moore, D. S., 2007. "Recent advances in trace explosives detection instrumentation". *Sensing and Imaging: An International Journal,* ***8***(1), pp. 9–38.

[3] Kuznetsov, A. V. and Osetrov, O. I., 2006. "Detection of improvised explosives (IE) and explosive devices (IED)". *Detection and Disposal of Improvised Explosives*, pp. 7–25.

[4] Ratner, S. B. and Korobov, V. I., 1965. "Self-heating of plastics during cyclic deformation". *Polymer Mechanics,* ***1***(3), pp. 63–68.

[5] Ratner, S. B., Korobov, V. I., and Agamalyan, S. G., 1972. "Mechanical and thermal fracture of plastics under cyclic strains". *Soviet Materials Science: A Translation of Fiziko-Khimicheskaya Mekhanika Materialov/Academy of Sciences of the Ukrainian SSR,* ***5***(1), pp. 66–70.

[6] Biot, M. A., 1958. "Linear thermodynamics and the mechanics of solids". *Proceedings of the Third US National Congress of Applied Mechanics, American Society of Mechanical Engineers*, pp. 1–18.

[7] Mignogna, R. B., Green, R. E., Duke, J. C., Henneke, E. G., and Reifsnider, K. L., 1981. "Thermographic investigation of high-power ultrasonic heating in materials". *Ultrasonics,* ***19***(4), pp. 159–163.

[8] Henneke, E. G., Reifsnider, K. L., and Stinchcomb, W. W. "Vibrothermography: Investigation, Development, and Application of a New Nondestructive Evaluation Technique". Technical Report AD-A175 373.

[9] Luo, W., Yang, T., Li, Z., and Yuan, L., 2000. "Experimental studies on the temperature fluctuations in deformed thermoplastics with defects". *International Journal of Solids and Structures,* ***37***(6), pp. 887–897.

[10] Chervinko, O. P., 2004. "Calculating the critical parameters characterizing the thermal instability of a viscoelastic prism with a stress concentrator under harmonic compression". *International Applied Mechanics,* ***40***(8), pp. 916–922.

[11] Renshaw, J., Chen, J. C., Holland, S. D., and Bruce, T. R., 2011. "The sources of heat generation in vibrothermography". *NDT&E International,* ***44***(8), pp. 736–739.

[12] Dimarogonas, A. D. and Syrimbeis, N. B., 1992. "Thermal signatures of vibrating rectangular plates". *Journal of Sound and Vibration,* ***157***(3), pp. 467–476.

[13] Katunin, A. and Fidali, M., 2011. "Experimental identification of non-stationary self-heating characteristics of laminated composite plates under resonant vibration". *Kompozyty,* ***11***(3), pp. 214–219.

[14] Katunin, A. and Fidali, M., 2012. "Self-heating of polymeric laminated composite plates under the resonant vibrations: Theoretical and experimental study". *Polymer Composites,* ***33***(1), pp. 138–146.

[15] Mares, J. O., Miller, J. K., Sharp, N. D., Moore, D. S., Adams, D. E., Groven, L. J., Rhoads, J. F., and Son, S. F., 2013. "Thermal and mechanical response of PBX 9501 under contact excitation". *Journal of Applied Physics,* ***113***(8), 084904.

[16] Miller, J. K. and Rhoads, J. F., 2013. "Thermal and mechanical response of particulate composite plates under direct excitation". *Proceedings of the ASME 2013 International Design Engineering Technical Conferences & Computers and Information in Engineering Conference; 25th Conference on Mechanical Vibration and Noise*, DETC2013-12138.

[17] Paripovic, J. and Davies, P., 2013. "Identification of the dynamic behavior of surrogate explosive materials". *Proceedings of the ASME 2013 International Design Engineering Technical Conferences & Computers and Information in Engineering Conference; 25th Conference on Mechanical Vibration and Noise*, DETC2013-12755.

[18] Wakashima, K. and Tsukamoto, H., 1991. "Mean-field micromechanics model and its application to the analysis of thermomechanical behaviour of composite materials". *Materials Science and Engineering: A,* ***146***(1), pp. 291–316.

[19] Arefinia, R. and Shojaei, A., 2006. "On the viscosity of composite suspensions of aluminum and ammonium perchlorate particles dispersed in hydroxyl terminated polybutadiene - New empirical model". *Journal of Colloid and Interface Science,* ***299***(2), pp. 962–971.

[20] Fu, S. Y., Feng, X. Q., Lauke, B., and Mai, Y. W., 2008. "Effects of particle size, particle/matrix interface adhesion and particle loading on mechanical properties of particulate–polymer composites". *Composites Part B: Engineering,* ***39***(6), pp. 933–961.

[21] Loginov, N. P., Muratov, S. M., and Nazarov, N. K., 1976. "Initiation of explosion and kinetics of explosive decomposition under vibration". *Combustion, Explosion, and Shock Waves,* ***12***(3), pp. 367–370.

[22] Loginov, N. P., 1997. "Structural and physicochemical changes in RDX under vibration". *Combustion, Explosion, and Shock Waves,* ***33***(5), pp. 598–604.
[23] Senchenkov, I. K., Karnaukhov, V. G., and Kozlov, V. I., 1986. "Toward a theory of governing equations of thermoviscoelasticity for periodic deformation". *Prikladnaya Mekhanika,* ***22***(8), pp. 97–104.
[24] Karnaukhov, V. G., 1993. "Modeling the oscillations and dissipative heating of inelastic bodies". *International Applied Mechanics,* ***29***(10), pp. 823–828.
[25] Senchenkov, I. K. and Karnaukhov, V. G., 2001. "Thermomechanical behavior of nonlinearly viscoelastic materials under harmonic loading". *International Applied Mechanics,* ***37***(11), pp. 1400–1432.
[26] Dinzart, F., Molinari, A., and Herbach, R., 2008. "Thermomechanical response of a viscoelastic beam under cyclic bending; self-heating and thermal failure". *International Applied Mechanics,* ***60***(1), pp. 59–85.
[27] Tschoegl, N. W., 1989. "The Phenomenological Theory of Linear Viscoelastic Behavior: An Introduction". *Springer-Verlag*.
[28] Jones, D. G., 2001. "Handbook of Viscoelastic Vibration Damping". *Wiley*.
[29] Brinson, H. F. and Brinson, L. C., 2008. "Polymer Engineering Science and Viscoelasticity: An Introduction". *Springer*.
[30] Markovitz, H., 1977. "Boltzmann and the beginnings of linear viscoelasticity". *Journal of Rheology,* ***21***(3), pp. 381–398.
[31] Rao, S. S., 2007. "Vibration of Continuous Systems". *John Wiley & Sons*.
[32] Timoshenko, S. P. and Goodier, J. N., 1951. "Theory of Elasticity". *McGraw-Hill*.
[33] Incropera, F. P., DeWitt, D. P., Bergman, T. L., and Lavine, A. S., 2007. "Introduction to Heat Transfer". *John Wiley & Sons*.
[34] Beck, J. V., Cole, K. D., Haji-Sheikh, A., and Litkouhi, B., 1992. "Heat Conduction Using Green's Functions". *Hemisphere Publishing Corporation*.
[35] Beer, F. P., Johnston, E. R., DeWolf, J. T., and Mazurek, D. F., 2009. "Mechanics of Materials". *McGraw-Hill*.
[36] Paripovic, J., 2013. Personal Communication.
[37] Paz, M., 1997. "Structural Dynamics: Theory and Computation". *Springer*.
[38] Gustafsson, S. E., 1991. "Transient plane source techniques for thermal conductivity and thermal diffusivity measurements of solid materials". *Review of Scientific Instruments,* ***62***(3), pp. 797–804.
[39] Rich, B. R., 1953. "An investigation of heat transfer from an inclined flat plate in free convection". *Transactions of ASME,* ***75***, pp. 489–499.
[40] Vliet, G. C., 1969. "Natural convection local heat transfer on constant-heat-flux inclined surfaces". *Journal of Heat Transfer,* ***91***(4), pp. 511–516.
[41] Goldstein, R. J., Sparrow, E. M., and Jones, D. C., 1973. "Natural convection mass transfer adjacent to horizontal plates". *International Journal of Heat and Mass Transfer,* ***16***(5), pp. 1025–1035.
[42] Tarver, C. M., Chidester, S. K., and Nichols, A. L., 1996. "Critical conditions for impact- and shock-induced hot spots in solid explosives". *The Journal of Physical Chemistry,* ***100***(14), pp. 5794–5799.
[43] Mattos, E. C., Moreira, E. D., Dutra, R. C. L., Diniz, M. F., Ribeiro, A. P., and Iha, K., 2004. "Determination of the HMX and RDX content in synthesized energetic material by HPLC, FT-MIR, and FT-NIR spectroscopies". *Química Nova,* ***27***(4), pp. 540–544.